



Full length article

Perfusion-decellularization of human ear grafts enables ECM-based scaffolds for auricular vascularized composite tissue engineering



Jérôme Duisit^{a,b,*}, Hadrien Amiel^a, Tsering Wüthrich^c, Adriano Taddeo^{c,d}, Adeline Dedriche^a, Vincent Destoop^e, Thomas Pardoën^e, Caroline Bouzin^a, Virginie Joris^a, Derek Magee^{f,g}, Esther Vögelin^d, David Harriman^h, Chantal Dessy^a, Giuseppe Orlando^h, Catherine Behets^a, Robert Rieben^c, Pierre Gianello^a, Benoît Lengelé^{a,b}

^a Institut de Recherche Expérimentale et Clinique (IREC), Université catholique de Louvain, Avenue Hippocrate 55/B1.55.04, B-1200 Brussels, Belgium

^b Department of Plastic and Reconstructive Surgery, Cliniques Universitaires Saint-Luc, Avenue Hippocrate 10, B-1200 Brussels, Belgium

^c Department for BioMedical Research, University of Bern, Murtenstrasse 50, CH-3008 Bern, Switzerland

^d Department of Plastic, Reconstructive and Hand Surgery, Inselspital, University Hospital, CH-3010 Bern, Switzerland

^e Institute of Mechanics, Materials and Civil Engineering, Materials and Process Engineering, Place Sainte Barbe 2/L5.02.02, B-1348 Louvain-la-Neuve, Belgium

^f School of Computing, University of Leeds, Leeds LS2 9JT, UK

^g HeteroGenius Limited, 21 Parkland Crescent, LS6 4PR Leeds, UK

^h Department of Surgery, Section of Transplantation, Wake Forest School of Medicine, 1 Medical Center Blvd, Winston-Salem, NC 27157, USA

ARTICLE INFO

Article history:

Received 26 October 2017

Received in revised form 27 March 2018

Accepted 4 April 2018

Available online 11 April 2018

Keywords:

Human

Ear graft

Perfusion-decellularization

Extracellular matrix

Vascularized composite tissue engineering

ABSTRACT

Introduction: Human ear reconstruction is recognized as the emblematic enterprise in tissue engineering. Up to now, it has failed to reach human applications requiring appropriate tissue complexity along with an accessible vascular tree. We hereby propose a new method to process human auricles in order to provide a poorly immunogenic, complex and vascularized ear graft scaffold.

Methods: 12 human ears with their vascular pedicles were procured. Perfusion-decellularization was applied using a SDS/polar solvent protocol. Cell and antigen removal was examined by histology and DNA was quantified. Preservation of the extracellular matrix (ECM) was assessed by conventional and 3D-histology, proteins and cytokines quantifications. Biocompatibility was assessed by implantation in rats for up to 60 days. Adipose-derived stem cells seeding was conducted on scaffold samples and with human aortic endothelial cells whole graft seeding in a perfusion-bioreactor.

Results: Histology confirmed cell and antigen clearance. DNA reduction was 97.3%. ECM structure and composition were preserved. Implanted scaffolds were tolerated *in vivo*, with acceptable inflammation, remodeling, and anti-donor antibody formation. Seeding experiments demonstrated cell engraftment and viability.

Conclusions: Vascularized and complex auricular scaffolds can be obtained from human source to provide a platform for further functional auricular tissue engineered constructs, hence providing an ideal road to the vascularized composite tissue engineering approach.

Statement of Significance

The ear is emblematic in the biofabrication of tissues and organs. Current regenerative medicine strategies, with matrix from donor tissues or 3D-printed, didn't reach any application for reconstruction, because critically missing a vascular tree for perfusion and transplantation. We previously described the production of vascularized and cell-compatible scaffolds, from porcine ear grafts. In this study, we applied findings directly to human auricles harvested from postmortem donors, providing a perfusable matrix that retains the ear's original complexity and hosts new viable cells after seeding. This approach unlocks the ability to achieve an auricular tissue engineering approach, associated with possible clinical translation.

© 2018 Acta Materialia Inc. Published by Elsevier Ltd. This is an open access article under the CC BY-NC-ND license (<http://creativecommons.org/licenses/by-nc-nd/4.0/>).

* Corresponding author at: UCL/SSS/IREC/CHEX, Avenue Hippocrate 55, mailbox B1.55.04, 1200 Brussels, Belgium.

E-mail addresses: jerome.duisit@uclouvain.be (J. Duisit), hadrien.amiel@student.uclouvain.be (H. Amiel), tsering.w@students.unibe.ch (T. Wüthrich), adriano.taddeo@dbmr.unibe.ch (A. Taddeo), adeline.dedriche@uclouvain.be (A. Dedriche), vincent.destoop@uclouvain.be (V. Destoop), thomas.pardoen@uclouvain.be (T. Pardoën), caroline.bouzin@uclouvain.be (C. Bouzin), virginie.joris@uclouvain.be (V. Joris), D.R.Magee@leeds.ac.uk (D. Magee), esther.voegelin@insel.ch (E. Vögelin), chantal.dessy@uclouvain.be (C. Dessy), gorlando@wakehealth.edu (G. Orlando), catherine.behets@uclouvain.be (C. Behets), robert.riegen@dbmr.unibe.ch (R. Rieben), pierre.gianello@uclouvain.be (P. Gianello), benoit.lengele@uclouvain.be (B. Lengelé).

<https://doi.org/10.1016/j.actbio.2018.04.009>

1742-7061/© 2018 Acta Materialia Inc. Published by Elsevier Ltd.

This is an open access article under the CC BY-NC-ND license (<http://creativecommons.org/licenses/by-nc-nd/4.0/>).

1. Introduction

Reconstruction of sizable auricular defects represents an enduring challenge in the field of plastic surgery, with variable clinical results despite extensive approaches and experimentation. Conventional autologous techniques [1–4] produce donor site morbidity and are limited by surgeon experience and expertise. The use of prosthetic cartilage implants has been reported, however the risk of extrusion has limited clinical applicability [5]. Vascularized Composite tissue Allotransplantation (VCA), whereby cadaver auricles are harvested and implanted into a recipient, are not available for single subunit reconstruction, since immunosuppressive (IS) treatment is not acceptable for such a small, non-life saving transplant [6]. In theory, tissue engineered (TE) autologous auricular implants may be able to overcome the limitations of current techniques [7–9], unfortunately the move from bench to bedside has yet to be achieved. Barriers to the success of TE auricles include the challenge of reproducing the biological complexity of human tissue along with the challenge of creating and accessing a vascular tree necessary for sustainment of seeded cells and implantation into a recipient. The perfusion-decellularization technique, as previously described in organs [10–14] and composite tissues [15–17], may represent the ‘holy grail’ of immunosuppression-free auricular transplantation. The basics of this technique involve circulating a mild detergent through a harvested organ/tissue via the native vascular system with the goal of removing cellular components, thus creating an extracellular matrix (ECM) scaffold retaining original tissue architecture and properties. The ECM scaffold could then be repopulated with autologous cells that would lead to a biological identity reassignment and immune tolerance once implanted. This technology appears ideally suited for the creation of a clinically useful bioengineered auricle. We previously reported the application of the perfusion-decellularization technique in porcine ear and human face models, with successful graft decellularization, preservation and accessibility of the vascular tree, suitable for repopulation with new cells and allocompatibility [18,19]. We hypothesized that this technology can be applied to human ear grafts. We hereby propose a method to process cadaveric human auricles, in order to provide a poorly immunogenic, complex and vascularized ear graft scaffold. Indeed, the relatively robust nature of composite tissues to post-mortem degradation could allow successful transplant processing, defining the new auricular synthesis approach of Vascularized Composite tissue Engineering (VCE).

2. Materials and methods

2.1. Specimens

Twelve ear grafts were harvested from eight human cadaveric donors at the Université catholique de Louvain human anatomy department (Brussels, Belgium). Prior to passing, all donors had consented to research and teaching on their body. Donors were aged 68–104 years at the time of death. Bodies were preserved at 4 °C for 1–4 days prior to graft procurement. All animal experiments were approved by the Université catholique de Louvain Animal Ethics Committee and following the EU Directive 2010/63/EU for animal experiments.

2.2. Ear graft procurement and perfusion-decellularization

According to previously described surgical protocol [20,21], ears were harvested with their corresponding vascular and nervous pedicles. Briefly, a peri-auricular incision was made within 1 cm around auricular implantation and continued to the temporal and cervical regions. In the cervical region, the common carotid artery,

external carotid artery, posterior auricular artery (PAA), proximal superficial temporal artery (STA), external jugular vein and great auricular nerve were isolated. All other arterial branches and collaterals were ligated. After temporal incision, distal STA and vein were identified and dissected distally to frontal and parietal branches. Pre-auricular STA dissection and exposure was completed through the parotid gland. Superficial temporalis fascia was incised circumferentially, then elevated by blunt subfascial undermining down to the zygomatic arch of the temporal bone aiming to reach the external acoustic meatus and posteriorly, to the external aspect of the mastoid process. During this retrograde dissection, the PAA was protected. Finally, the ear was completely elevated, along with its pedicle. Contralateral ear was either harvested identically or simply explanted as control. A luer was inserted in the arterial pedicle for heparinized saline (15 UI/ml) irrigation of the graft. This solution was infused until clear return was identified, in veins left free. Complementary vascular control was performed with either suture ligation or microclips. Remaining parotid tissue was excised then each ear was weighted. The arterial catheter was then connected to a Masterflex L/S peristaltic pump with L/S easy load pump head and L/S 16G tubing (Cole-Palmer Instrument Co, Vernon Hills, IL, USA) after final immersion in a 1L glass jar filled with the same solution as perfused. Perfusion-decellularization sequence, in an open circuit fashion, followed eight steps: (1) 1000 ml of heparinized saline (15UI/ml), containing 10 µM adenosine (Sigma-Aldrich, St. Louis, MO), 4 °C; 1% sodium dodecyl sulfate (SDS, VWR, Radnor, PA) in deionized water (DIW) was perfused for 88 h (36500 ml), room temperature (RT). This treatments leads to epidermolysis and bullae formation, tissue bleaching and edema formation, while shape is preserved; (2) DIW was then perfused for 3 h (1200 ml), RT; (3) Triton-X 100 1% (VWR) in DIW for 25 h (10000 ml), RT; (4) Phosphate buffered saline (PBS) for 38 h (16000 ml), RT; (5) Polar solvent step (100% 2-propanol, VWR), as previously described [22,23], whereby the flap was perfused for 4 h (1000 ml), until critical increase of vascular resistances, then transferred to a stirring bath of polar solvent overnight at RT, changed once, then rinsed in DIW bath for 2 h, and finally perfused with PBS for 30 h (16000 ml). This treatment removes oil from adipose tissue layer; (6) Type I Bovine DNase (Roche I, Sigma), 50 UI/ml in PBS with 203.3 M magnesium chloride (Sigma), for 6 h (900 ml), 37 °C; (7) final wash of the auricle with PBS for 12 h (4500 ml), RT. For all steps flow rate was set between 6 and 8 ml/min, in order to observe a mean arterial pressure (MAP) under 80 mmHg, with exception of DNase 2 ml/min perfusion. Decellularized human ears (HE-ECM) were stored at 4 °C in PBS. Before tissue analysis, each HE-ECM was weighted, examined for epidermis and hair remnants, bleaching and morphology.

2.3. Arterial pressure monitoring

During all steps of perfusion-decellularization, with exception of polar solvent perfusion, MAP was recorded with a central line connected to a Datex-Ohmeda S/5 anesthesia monitor and M-Prestin module (GE Healthcare Life Sciences, Chicago, IL, USA) for a selected pump inflow. A MAP profile was established for a constant flow of 8 ml/min.

2.4. Fluoroscopic vascular assessment

Contrast agent (Visipaque, GE Healthcare) mixed with normal saline (1:2) was injected in the arterial pedicle by a constant manual syringe pressure, for a HE-ECM scaffold compared to a native ear graft. Image acquisition was performed with a Powermobil C-Arm (Siemens, Munich, Germany). Images were exported in DICOM format and visualized with Osirix© software (Pixmeo, Bernex, Switzerland).

2.5. Histology, immunohistochemistry (IHC), immunofluorescence (IF)

Paraffin-embedding

Tissues were fixed in 4% formalin for 24 h, transferred in successive toluene and alcohol baths prior to dehydration, then embedded in paraffin and sectioned into 5 μm slices.

Histological staining

Sections were deparaffinized and rehydrated. We used hematoxylin and eosin (H&E), Masson's trichrome (MT), alcian blue and safranin O stains according to standard protocols. Miller's elastin/alcian blue/sirius red stains were also performed as described [24] in order to stain elastic fibers (purple), sulfated glycosaminoglycans (GAGs) (blue) and collagen (red).

IHC

After deparaffinization, slides were subjected to antigen retrieval by heating at 98 °C for 60 min in 10 mM citrate buffer, at pH 5.7. Endogenous peroxidases were inhibited using 1% H_2O_2 and non-specific antigenic sites were neutralized with 1:50 goat serum. Samples were incubated at 4 °C overnight, using the primary antibodies: anti-MHC type I + HLA A + HLA B (ab134189, 1:200, Abcam, Cambridge, UK) and anti-CD31 (ab28364, 1:50, Abcam). Next, the sections were incubated with 1:50 biotinylated secondary antibody, stained with streptavidin-HRP (Sigma) and 3,3'-diaminobenzidine (DAB) peroxidase substrate (Vector laboratories, Burlingame, Ca, USA), followed by counterstaining in Mayer's hematoxylin for 1 min, dehydration in alcohol and toluene baths and finally mounting with Entellan mounting medium. PBS containing 1% bovine serum albumin (BSA) was used to rinse sections after each step.

IF

Deparaffinized, formalin-fixed sections were quenched with NaBH_4 (1:100), then subjected to antigen retrieval by heating at 98 °C for 60 min in 10 mM citrate buffer, pH 5.7. Samples were incubated at 4 °C overnight with the following primary antibodies: anti-type I collagen (ab34710, 1:250, Abcam), anti-type II collagen (ab34712, 1:200, Abcam) and anti-type IV collagen (ab6586, 1:500, Abcam). Neutralization of nonspecific sites was done with PBS containing 5% BSA. For fluorescence staining, secondary antibody labeled with Alexa Fluor 488 (goat anti-Rabbit or anti-mouse IgG, 1:300, ThermoFisher Scientific, Waltham, MA), was used and the nuclei were stained with 4'-6-diamidino-2-phenyl-indole (DAPI, 1:1000) and mounted with DAKO fluorescent mounting medium (Agilent, Santa Clara, CA, USA).

Lipid droplet evaluation on frozen sections

Tissue-Tek O.C.T. Compound (Sakura Finetek, Alphen aan den Rijn, The Netherlands) embedded biopsies were cut on a Microm HM 560 cryostat (ThermoFisher). Sections were cut to 5 μm thickness and processed for the staining. For type IV Sudan staining, sections were fixed for 10 min in 4% formaldehyde directly after thawing, washed, incubated for 30 min in a Sudan IV saturated solution, washed and mounted.

Histology and IHC sections were digitalized at 40 \times magnification with a SCN400 slide scanner (Leica, Wetzlar, Germany) and visualized using Digital Image Hub (Leica Biosystems, Dublin, Ireland). Images of IF sections were acquired on a Zeiss AxioImager.z1 fluorescence microscope (Zeiss).

2.6. 3D-histology serial reconstruction and analysis

Full-thickness biopsies were taken from a native ear and a HE-ECM graft. For each sample, 50 serial sections of 5 μm thickness were prepared with Miller's elastin/alcian blue/sirius red stains.

Slides were scanned using the SCN400 slide scanner (Leica) with a 40 \times objective. Damaged sections were discarded after visual examination (2–3 sections per sample) and 3D-reconstruction was performed using the HeteroGenius MIM 3D Pathology add-on (HeteroGenius Ltd, Leeds, UK) with 4 levels of non-rigid alignment (1.25 \times , 2.5 \times , 5 \times and 10 \times) and a final B-Spline size of 12 \times 12 mm, subsequent to automatic rigid alignment of sections performed at 1.25 \times . Whole sample 3-D visualization of original data (~1000 \times 1000 \times 50 voxels) was produced, with a total volume of 7.61 mm³ and 8.21 mm³ in the native ear and HE-ECM graft samples respectively. Subvolume analysis data, defined by volumes of interest in the cartilage, skin and connective tissue, from both native and decellularized samples, was annotated manually on a single slide, using a box of approximately 1 \times 1 \times 0.25 mm. Animated Graphics Interchange Format (GIF) images of the whole stack were produced by exporting the aligned stack volumes from HeteroGenius MIM and using ImageJ software [25] for volume rendered examples.

Quantitative analysis of porosity was performed on tissue samples using the HeteroGenius MIM Colour Analysis add-on. A 3-class (collagen, elastin and background) probabilistic model was built by manually labelling examples of each class. Pixel counting for each class was performed for a single annotated sub-region per image, by classifying a pixel as belonging to the class if the probability of class membership was 0.75 or larger ("QuantifyByColour" analysis method). Annotation of the tissue region was performed automatically at 0.625 \times resolution, which uses a greyscale threshold (value = 200), plus morphology, hole filling and boundary tracing to annotate tissue pieces with a Bezier curve. Porosity was obtained by the ratio between non-stained and stained volumes between a native and a decellularized serial-sectioned samples. Additionally, annotations excluding the cartilage were produced manually for a subset of 2 images per sample.

2.7. Scanning electron microscopy (SEM)

Native and decellularized biopsies were fixed with 2.5% glutaraldehyde overnight at 4 °C. Samples were then washed with PBS and gradually dehydrated by successive immersion in increasing concentrations of ethanol for 15 min each. Before SEM imaging, tissues were critical-point dried and coated with an 8-nm gold layer. SEM measurements were performed at 15 keV. Samples were observed with a field-emission scanning electron microscope (JSM-7600F, Jeol, Akishima, Tokyo, Japan) according to standard protocols.

2.8. DNA quantification

DNA of skin (n = 6), fat (n = 4) and cartilage (n = 3) samples from native ear (n = 3) and HE-ECM (n = 3) was extracted, with DNeasy Blood & Tissue Kit (Qiagen, Hilden, Germany), processing up to 25 mg biopsies. Briefly, tissues were incubated overnight at 56 °C with proteinase K (40 mAU/mg protein) solution. After adding buffer and ethanol, the mixture was transferred to a spin column filled with buffers and repeated elution was performed. Extracted DNA content was assessed by Quant-it™ Picrogreen dsDNA assay kit (ThermoFischer Scientific), according to manufacturer's protocol. Final value was expressed in ng DNA per mg tissue wet weight.

2.9. ECM protein quantification

Biopsies of skin (n = 6), fat (n = 4) and cartilage (n = 3) samples from native (n = 3) and decellularized (n = 3) different ear grafts were used. Collagen content was evaluated using a Chondrex hydroxyproline assay kit (Chondrex, Inc., Redmond, WA) according to manufacturer's protocol. Briefly, samples were hydrolyzed in

10 M hydrochloric acid for 24 h at 100 °C, and mixed with hydroxyproline standards. Chloramine-T was added to solution from samples and standards, then incubated 20 min at room temperature. DMAB was added to standards and samples solutions, then incubated at 60 °C. Absorbance was read at 570 nm. *GAGs content* was evaluated using the Blyscan Sulfated-GAG assay kit (Biocolor LTD, Carrickfergus, Northern Ireland) according to manufacturer's recommendations; samples extraction was preceded with papain overnight at 65 °C. After centrifugation, supernatant was collected and color reactant was added to precipitate S-GAGs, followed by repeated centrifugation until dissociation was completed. Standard was bovine tracheal chondroitin 4- sulfate. Absorbance was read at 630 nm. *Elastin content* was measured with the Fast Elastin Assay kit (Biocolor) according to manufacturer's recommendations. 0.25 M oxalic acid was added to samples, and digested for one hour at 100 °C before supernatant collection. This extraction was repeated two times for skin and fat and three times for cartilage and muscle. Final extraction volume was mixed with equal reactant volume for elastin precipitation until complete elastin digestion and centrifuged. Colored reactant was added in the remaining solution, stirred and centrifuged prior to supernatant elimination. Standard was a high molecular weight fraction of α -elastin prepared from bovine neck ligament elastin in oxalic acid. Absorbance was read at 510 nm. All results were expressed as $\mu\text{g}/\text{mg}$ wet weight.

2.10. Mechanical properties

We used an Instron-5666 universal testing machine (Instron Corporation) for all experiments. Ball burst tests were performed to determine the stiffness of the cartilage. A 4-mm diameter steel ball with 1 mm/min loading rate, and a 100 N load cell, was applied to decellularized ($n = 5$) and native ($n = 5$) disc samples each from a different donor, clamped in 5-mm diameter O-rings. Endpoint was the maximum force. Stiffness was expressed as the ratio between the maximum force and the corresponding crosshead displacement. Values were divided by sample thickness and expressed as N/mm.

Tensile tests were performed to determine the stress-strain response of native ($n = 4$) and decellularized ($n = 6$) skin samples, originated from different donors. Rectangular cross section samples were submitted to a tensile load with a 1 mm/min crosshead speed and a 20 mm initial grip distance.

2.11. Cytokines quantification

Protein extraction

Skin, cartilage and fat tissue biopsies were collected from native ($n = 4$) and decellularized ear grafts ($n = 3$). Samples were kept at 4 °C until processing. Biopsies were weighed on an analytical scale and cut into small pieces with a surgical knife. The pieces were transferred into M tubes (Miltenyi Biotec GmbH, Bergisch Gladbach, Germany) containing RIPA buffer (50 mM Tris-HCl, pH 8.0, with 150 mM sodium chloride, 1.0% Igepal CA-630 (NP40), 0.5% sodium deoxy cholate and 0.1% sodium dodecyl sulfate) laced with protease inhibitor cocktail (P8340, 1:100, SIGMA). M tubes were promptly inverted and put on a gentle MACS Dissociator (Miltenyi Biotec GmbH), then homogenized using the program specific for protein extraction. After termination of the program, homogenates were incubated on ice and underwent sonication. After a short spin down, the supernatant was transferred to smaller tubes for centrifugation at 13'000 rpm for 1 h at 4 °C. Again, the supernatant was transferred to a new tube for further analysis. For protein quantification, a classical Bicinchoninic acid (BCA) assay was performed. A bovine serum albumin standard (2.0 mg/ml in 0.9% aqueous NaCl containing sodium azide, 23209, Thermo Fisher Sci-

entific) was prepared and transferred to a flat transparent 96-well plate (Thermo Fisher Scientific). 5 μl of sample were added to the wells and the assay was performed according to the DC Protein Assay kit instructions (Bio-Rad, Hercules, CA, USA). The OD was measured at 750 nm on a plate reader (Infinite M1000 PRO) and interpolated by Prism 7 (GraphPad Software, La Jolla, CA, USA).

Cytokine measurement

Protein levels of 42 different cytokines were measured by Bio-Plex multiplex immunoassays. The Bio-Plex Pro Human Chemokine 40-Plex Panel (Bio-Rad) and the Bio-Plex Pro TGF- β 3-Plex kit (Bio-Rad) were used to analyze the supernatants of the protein extraction (above) and run on a FLEXMAP 3D system (Luminex, Austin, CA, USA). The procedure was performed based on the original manufacturer instruction manual. Growth factor content was normalized to the mass of starting tissue and expressed as pg of analyte per mg of tissue. After log₂ transformation, concentrations above or below the limit of detection were eliminated from the analysis.

2.12. In vivo biocompatibility study

16 adult Wistar rats (all females, mean weight 208 ± 15 g) were implanted subcutaneously with 2 biopsies, helix and lobe of approximately $7 \times 7 \times 3$ mm, from either native ear ($n = 8$) or HE-ECM ($n = 8$), previously sterilized by 0.1% peracetic acid (PCA). Samples came from three different donors in each group (control versus decellularized). Within each group, we used the same three different donors for each period of sacrifice (day 15, day 30, day 60 – with exception of this last group involving only two different donors. General anesthesia was performed using intra-peritoneal injection of 50 mg/ml Ketamine with 20 mg/ml Xylazine in saline. After disinfection, a median incision was performed on the abdomen and two subcutaneous pockets were created. For serum collection, 1 ml blood puncture was performed at time of implantation and sacrifice; collected blood was then centrifuged 15 min at 3000 rpm, and serum preserved at -80 °C. Euthanasia was performed at postoperative day (POD)15 ($n = 6$), POD30 ($n = 6$) and POD60 ($n = 4$); then implants were retrieved, paraffin-embedded, sectioned and stained with H&E, MT, anti-CD68 (ab31360, Abcam) and anti-CD3 (ab16669) with IHC. For inflammatory and lymphocytic quantification, CD68- and CD3-stained sections were digitalized with the slide scanner and analyzed using the image analysis tool (Author version 6.6.3, Visiopharm, Hørsholm, Denmark). The implant in each section was delineated manually and care was taken to exclude tissue folds and artefacts from the analysis. CD68- and CD3-positive pixels were then detected within the previously delineated tissue at high resolution ($20\times$) using a classification based on image feature highlighting the DAB staining (HDAB-DAB matrix of the software). Threshold was adjusted on representative stained vs non-stained tissue areas. The results were expressed as CD68- and CD3-stained area percentages and calculated as-stained area/total tissue area $\times 100$. The parameters were kept constant for all slides.

Detection of anti-donor alloantibody (IgG) by flow cytometry

Human peripheral blood mononucleated cells (PBMC), freshly taken from a healthy donor, were incubated with recipient serum for 30 min at room temperature. Before incubation, the serum was decomplexed for 30 min at 56 °C. After washing with fluorescence-activated cell sorting buffer (Hanks balanced salt solution – HBSS – containing 0.5% fetal bovine serum and 0.1% sodium azide), saturating amounts of Alexa Fluor 488 goat anti-rat IgG polyclonal antibody (Thermo Fisher Scientific, Merelbeke, Belgium) was added and incubated for 30 min at room temperature, then washed twice. Each analysis included the appropriate

Alexa Fluor 488-conjugated antibody with only PBMCs, for non-specific reaction. Cells were acquired and analyzed with BD FACScalibur (BD Bioscience Benelux NV, Erembodegem, Belgium) driven by CellQuest Pro software (BD Bioscience). A positive reaction was defined as a shift of more than 10-channels in mean fluorescence intensity when testing donor lymphocytes with post-transplantation (Day 15, 30 and 60) serum and comparing with pre-transplant serum (Day 0).

2.13. Scaffold seeding with rodent adipose-derived stem cells

Rat Adipose-derived stem cells (rASCs)

rASCs were isolated as previously reported [26]: briefly, we retrieved fresh inguinal fat from one adult rat, right after euthanasia for other experiments. Fat was digested with type II collagenase (LS004176, Worthington, Lakewood, NJ, USA), reconstituted in HBSS, and incubated for 1 h at 37 °C with continuous agitation for 60 min. After digestion, the collagenase was inactivated in Dulbecco's Modified Eagle's Medium (DMEM, Westburg, Leusden, The Netherlands) supplemented with 10% FBS, 2 mM L-glutamine, penicillin 100 U/mL, and streptomycin 100 µg/mL. Collected tissue was centrifuged for 10 min at 1500 rpm, at room temperature. The supernatant was aspirated and cells pellet was suspended with DMEM with 10% FBS, 2 mM L-glutamine, penicillin 100 U/mL, and streptomycin 100 µg/mL. After filtration through a 500-µm mesh screen, the collected tissue was centrifuged for 10 min at 1500 rpm, at room temperature and the pellet was suspended in proliferation medium and identified as the stromal vascular fraction (SVF). After 24–48 h of incubation at 37 °C in 5% CO₂, the cultures were washed with PBS and maintained in proliferation medium, containing DMEM with 4.5 g/L glucose w/o L-Glutamine supplemented with 10% of FBS, 1% of P/S and 1% of Glutamine and trypsinized when reaching 80% confluence, up to 4 passages.

Scaffold sample seeding

Decellularized HE-ECM samples (n = 9), from external carotid artery pedicle (D-Artery, n = 2), dorsal skin (D-Skin, n = 2) and helix full-thickness (D-FT, n = 4) biopsies, were sterilized: briefly, 0.1% PCA (Sigma) was prepared with DIW, and sterilized with a filtration unit. Samples were then washed overnight in PCA, using an orbital stirrer. Samples were then rinsed with DIW and repeated PBS washes on orbital-shaker, and finally preserved in sterile PBS/AA. Scaffolds were positioned in a 24-well plate, then impregnated with supplemented DMEM (10% of FBS, 1% of P/S and 1% of Glutamine). rASCs were seeded at a density of 3.6×10^4 cells/cm² on each scaffold. All seeded HE-ECM were then placed in a CO₂ incubator, and cultivated under standard conditions. Medium was changed every 48 h for 14 days. At retrieval, biopsies were first treated as whole-mounts with vital staining then Vybrant MTT (4,5-Dimethylthiazol-2-yl)-2,5-Diphenyltetrazolium Bromide) Cell Proliferation Assay Kit (Life Technologies) was used, mixing 12 mM MTT with PBS. Next, specimens were incubated with scaffold for 4 h at 37 °C observed under a binocular microscope, and with Live/Dead Viability/Cytotoxicity Kit (Life Technologies, L3224), incubating 2 mM ethidium homodimer and 4 mM calcein-AM with samples for 40 min at room temperature. The rest of the constructs were paraffin-embedded, sectioned and stained with H&E.

2.14. Bioreactor whole-graft human aortic endothelial cells (HAEC) seeding

Scaffold preparation

A whole HE-ECM graft was sterilized using 0.1% PCA protocol of alternating bath-stirring and perfusion, under sterile conditions, as previously described [18]. The HE-ECM was then mounted in a

sterile perfusion-bioreactor, in closed circuit with the arterial pedicle connected to the tubing and the veins left free in the jar. The perfusion chamber was filled with 900 ml DMEM and graft conditioned for 2 h with perfusion set at 5 ml/min, in a CO₂ incubator, set at 37 °C and 5%CO₂.

HAEC isolation and culture

Purchased HAEC ((304-05A, Sigma-Aldrich) were cultivated on 0.2% gelatin (Sigma G1393), with Endothelial Cell Growth Medium MV2 (Bio-Connect, Toronto, Canada), changed twice a week, and cells amplified 6 times once a week (standard passage) until passage four.

Bioreactor whole-scaffold vascular seeding and culture

After scaffold immersion in 500 ml Endothelial Cell Growth Medium MV2, 30×10^6 HAEC suspended in 7 ml medium were slowly injected through the arterial line. After a four-hours static period, to allow endothelial cell attachment, the perfusion flow was restarted at 2 ml/min overnight, then increased to 6 ml/min. After 48 h, the culture was stopped; biopsies were processed for Live/Dead, MTT and CD31 IHC stainings.

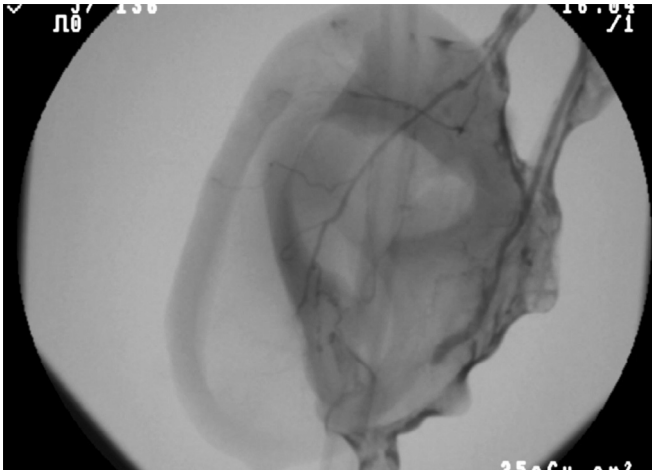
2.15. Statistical analysis

Graphic presentation and statistical analysis was performed on Prism 7 (GraphPad Software). For GAGs, elastin and collagen content, unpaired student t-tests were performed between native and decellularized ear samples. For cytokines, two-sample t-tests with Benjamini, Krieger and Yekutieli correction were performed to quantitatively compare their abundance in native and decellularized tissues. One-way ANOVA with post-hoc Tukey's multiple comparison correction was used to compare the relative preservation of the different cytokine groups within the analyzed tissues. Data are presented as mean ± SEM for all analysis with exception of cytokines quantification expressed as mean ± SD. P < 0.05 was considered statistically significant.

3. Results

3.1. Perfusion-decellularization

Blistering was observed within the first 12 h of SDS perfusion, first affecting the posterior surface followed by the anterior surface of the graft. The blisters evolved into large bullae which led to complete epidermis removal (Fig. 1A and B). After completion of the Triton-X step, a yellowish aspect of the adipose tissue remained, demonstrating scattered oil cysts. Adipose tissue was satisfyingly treated after the supplementary 2-propanol step, as confirmed by macroscopic observation and type IV Sudan staining (Fig. 1C and D). After the final PBS step, the cartilage layer retained the original auricular morphology. Arterial vascular patency was confirmed by fluoroscopy (n = 2), with opacification of ECA, PAA and STA axis and their distal parenchymal branches, without signs of intra-graft contrast extravasation (Fig. 1E, Supplementary Video 1). Venous outlet couldn't be assessed with this analysis: the liquid drops observation only reflected the quality of the venous vascular control at graft section, more difficult in decellularized ears, with however no impact on the quality of the decellularization and the patency of the vascular tree; the venous obstruction, correlated to parenchyma edema formation, was very limited. Regarding MAP evolution during protocol, SDS perfusion was associated with an important increase of arterial vascular resistances, macroscopically associated with edema of the fat layer; MAP decreased as steps were followed, and finally came back to initial MAP value after decellularization completion (Fig. 1F).



Supplementary Video 1.

3.2. Cell clearance

H&E and DAPI confirmed cellular clearance in skin and adnexa, with a few remnant chondrocyte nuclei visible in the deep cartilage, associated with negativity of type I MHC markers in treated

grafts (Fig. 2A–C). The complete nuclei clearance could be observed already before DNase perfusion (see Supplementary material 2). CD31 markers of endothelial cells were also completely removed (Fig. 2D). DNA quantifications in D-Skin, D-Fat and D-Cartilage were found to be respectively 0.99 ± 0.75 , 0.84 ± 0.56 and 4.82 ± 3.95 ng/mg wet weight compared to 88.7 ± 9.6 , 28.2 ± 15.7 and 121.7 ± 31.1 ng/mg wet weight in native samples; this represented an overall 97.3% DNA reduction in HE-ECM ($p < 0.001$) (Fig. 2E).

3.3. ECM preservation

3.3.1. Histology

MT, type I and type II collagen stains confirmed the high-quality preservation and structural organization of major collagen proteins (Fig. 3A–C). Type IV collagen, which is fundamental for basal membranes and critical for further epidermal reconstruction strategies, was well-observed in the vessels, glands and especially in the dermis, at the level of the dermo-epidermal junction (DEJ) (Fig. 3D). Alcian blue and safranin O stains demonstrated GAG preservation in the cartilage layer, with some reduction in peripheral areas more exposed to the decellularizing flow agents through the perichondrium (Fig. 3E and F).

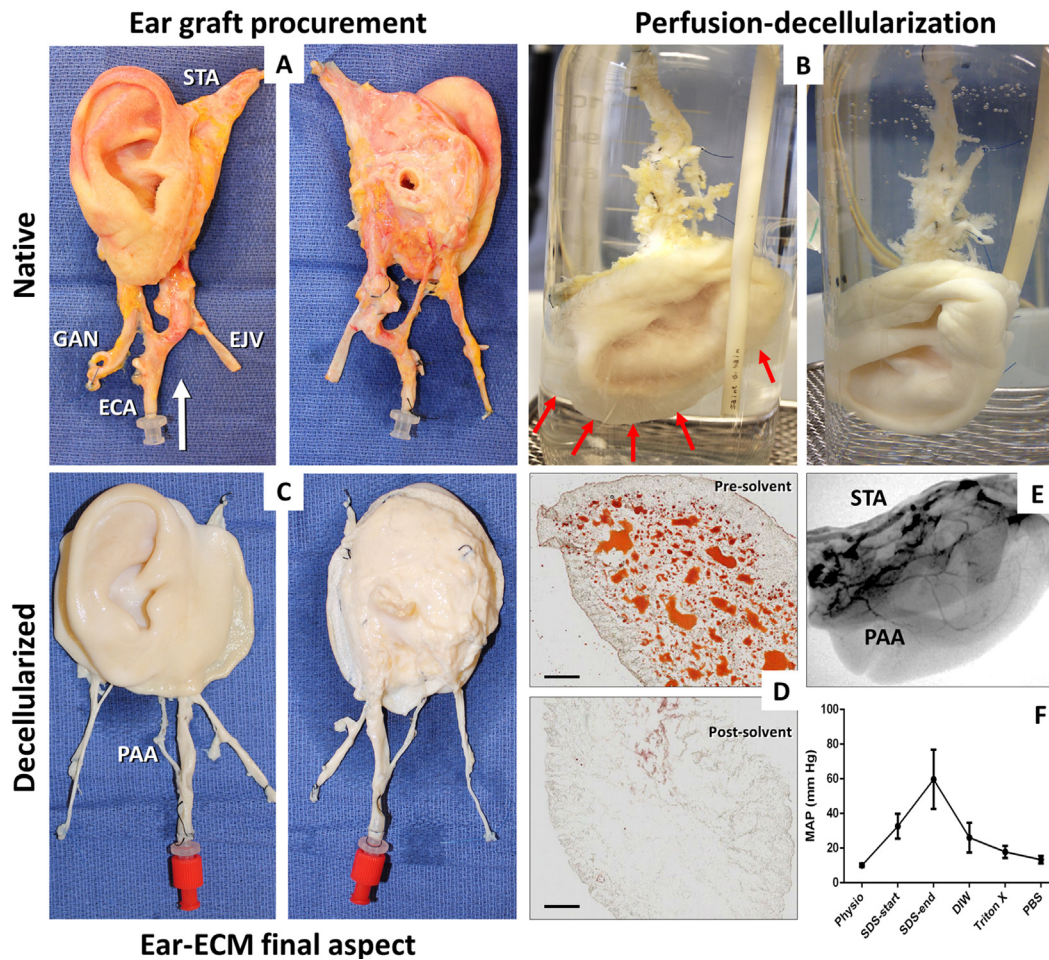


Fig. 1. Cadaveric ear graft perfusion-decellularization. **A** Native ear flap after procurement, with arterial (external carotid artery ECA, posterior auricular artery PAA, superficial temporal artery STA) and venous (external jugular vein EJV) pedicle, with anterior (left) and posterior (right) views; the arrow indicates the flow direction. **B** Perfusion-decellularization: left, after 24 h perfusion, with evidence of epidermolysis and large bullae formation (arrows); right, final aspect. **C** Decellularized ear anterior (left) and posterior (right) views, with evidence of morphology preservation and oil cysts removal, after 2-propanol solvent treatment. GAN Great Auricular Nerve. **D** Ear lobe section and staining with type IV Sudan fat staining prior (up) and after (down) polar solvent treatment. Scale bars 1 mm. **E** Arterial fluoroscopy of decellularized ear: STA and PAA are opacified. **F** Mean arterial pressure (MAP) evolution during process ($n = 4$), at constant output. MAP expressed in mm Hg.

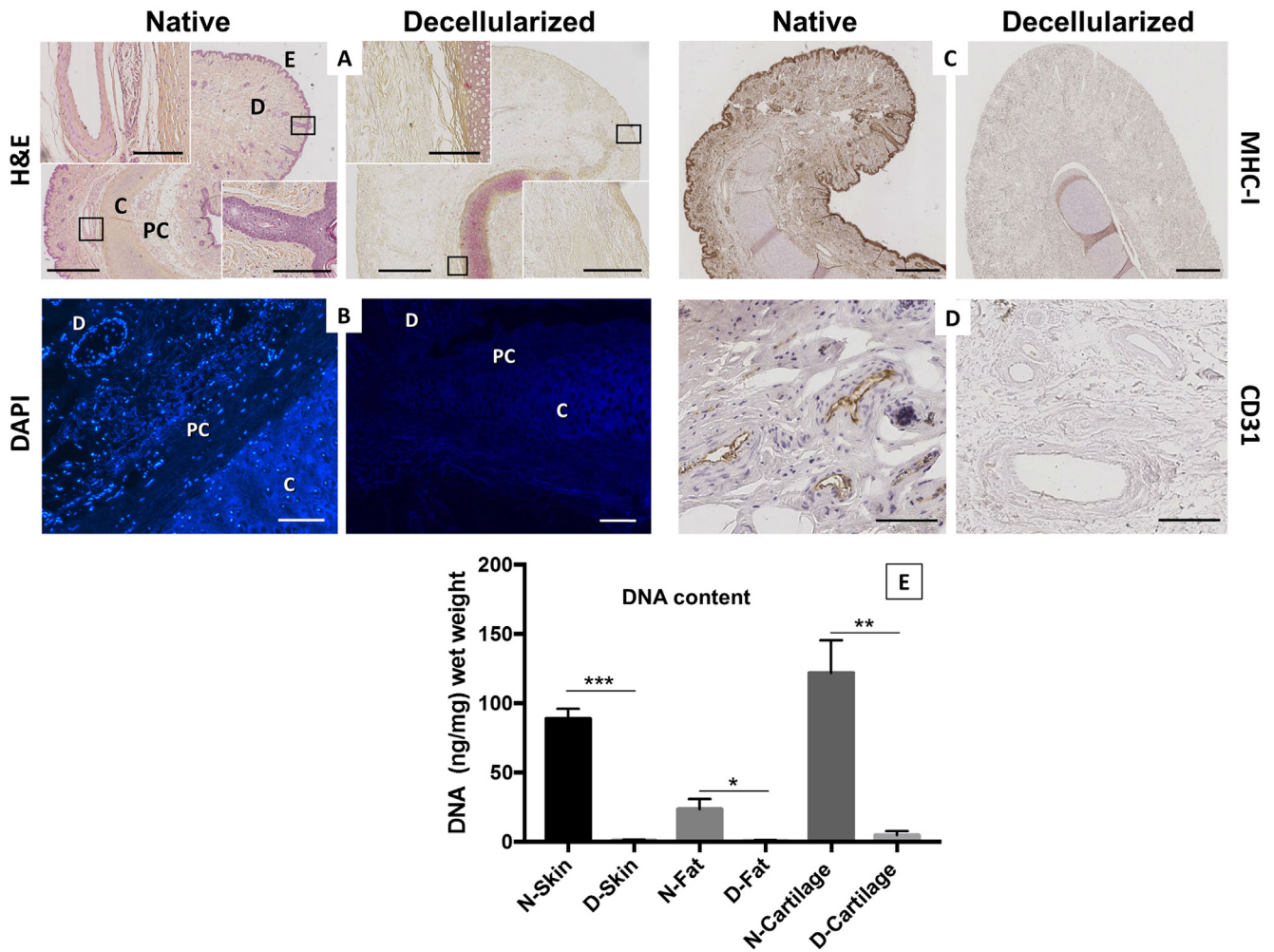


Fig. 2. Cells and antigens removal. **A** H&E staining comparing native (left) and decellularized (right) ear grafts. E epidermis, D dermis, PC perichondrium, C cartilage. Inserts show magnified details (black squares) of the section. **B** DAPI staining showing native (left) and decellularized (right) ear sections. **C** anti-type I HLA staining in native (left) versus decellularized (right) tissues. **D** Anti-CD31 staining in native (left) versus decellularized (right) tissues. **E** DNA content in native (N-) versus decellularized (D-) tissues, expressed in ng/mg wet weight. Analysis performed on skin (n = 6), fat (n = 4) and cartilage (n = 3) samples from native ear (n = 3) and HE-ECM (n = 3). Statistics were performed using unpaired student *t*-test, mean \pm SEM, ****p* < 0.001, ***p* < 0.01, **p* < 0.05. Scale bars: upper row, 1 mm for the section overview, 200 μ m for the inserts; lower row 100 μ m.

SEM examination reveals the preservation of the HE-ECM ultrastructure with dermal papillae, cartilage with emptied chondrocyte lacunae, and fat with fibrillary organization and absence of oil cysts. No detergent crystal could be detected in examined samples, revealing the efficiency of PBS perfusion to remove them (Fig. 3G–J).

3.3.2. ECM protein quantification

The qualitative ECM assessment was correlated to the preservation of its major protein content (Fig. 3K–M). Collagen was highly preserved in D-Skin, D-Fat and D-Cartilage (87.2 ± 14.3 , 126.5 ± 52.5 and 36.7 ± 12.3 μ g per mg wet weight respectively) compared to controls (20.3 ± 8.2 , 41.2 ± 23.2 and 21 ± 8 μ g per mg wet weight respectively), representing a mean relative increase in collagen content of 300% compared to native tissues. The global content increase is explained by collagen preservation following perfusion-decellularization, as well as by the reduction of cell content and other ECM proteins, leading to an important relative mass increase in all ear scaffold tissues. Mean elastin content in D-Skin, D-Fat and D-Cartilage was 4.96 ± 1.5 , 3.96 ± 0.99 and 13.64 ± 1.8 μ g per mg wet weight respectively, compared to 16.68 ± 4.41 , 14.53 ± 6.44 and 14.98 ± 6.92 μ g per mg wet weight respectively

in controls. Reduction of elastin was significant in skin ($p < 0.05$), with 41.3% relative preservation of elastin content while in cartilage 82% of native elastin content was preserved with non-significant difference. For GAGs, D-Skin, D-Fat and D-Cartilage was 0.2 ± 0.1 , 0.33 ± 0.01 and 2.82 ± 1.2 μ g per mg wet weight respectively, compared to 0.53 ± 0.01 , 0.47 ± 0.11 and 7.23 ± 0.65 μ g per mg wet weight respectively in controls. D-Skin preserved 42.6% of native GAG content while GAG value represented 40% of native content preservation for D-Cartilage ($p < 0.05$). It is vitally important that both elastin and collagen content are preserved in cartilage, as they are primarily responsible for the mechanical properties of cartilage: indeed, preservation of the morphological support is one of the most important feature for auricular graft functionality.

3.3.3. The tridimensional structural preservation

The tridimensional structural preservation of specific elements of the composite tissue is appreciated (elastin, collagen, GAGs), by the 3D-ECM histological reconstructions. From these samples, we extracted a volume of subunits for 3D reconstructions (Fig. 4A and B), enabling a better targeted structural assessment. The 3D cartilage subunit evaluation confirmed the 2D histology observation and quantification, with a better characterization of

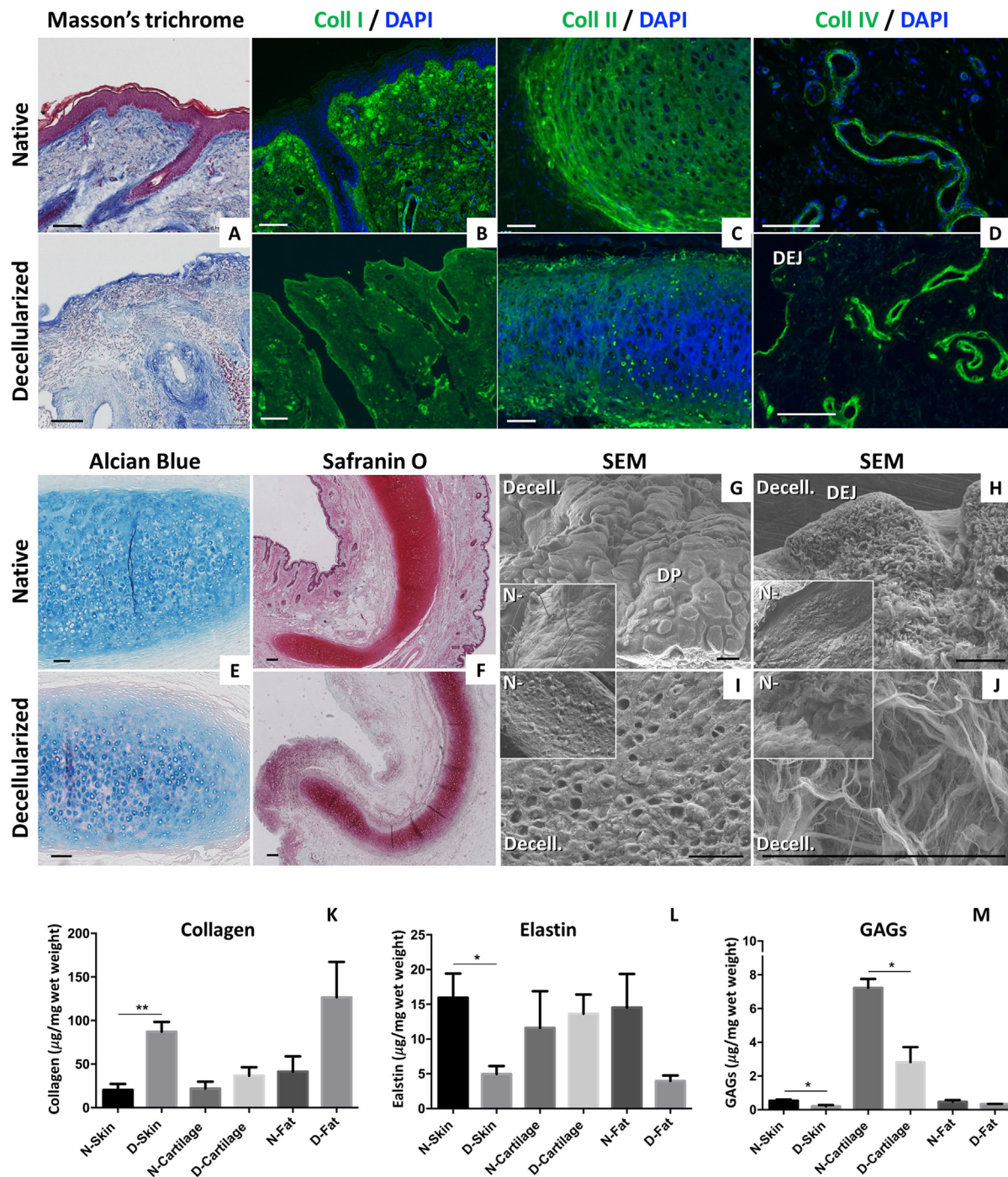


Fig. 3. ECM major proteins and 2D structure preservation. **A–F** Histology stainings by **A** Masson's trichrome of skin, **B** Type I collagen of skin, **C** type II collagen of cartilage, **D** type IV collagen in dermis, **E** Alcian blue and **F** Safranin O in cartilage, of native (upper row) and decellularized (lower row) tissues; DEJ, dermo-epidermal junction. **G–J** SEM evaluation of **G** dermal surface with preserved dermal papillae (DP), **H** dermal section with appreciation of DEJ, **I** cartilage section and **J** adipose tissue, from acellular scaffolds; insert represent native samples. **K–M** Major ECM content quantification: **K** Collagen, **L** Elastin and **M** GAGs; expressed in µg/mg wet weight of tissue. Analysis performed on skin (n = 6), fat (n = 4) and cartilage (n = 3) samples from native ear (n = 3) and HE-ECM (n = 3). Statistics were performed using unpaired student *t*-test, mean ± SEM, ***p* < 0.01, **p* < 0.05. Scale bars: 100 µm. (For interpretation of the references to color in this figure legend, the reader is referred to the web version of this article.)

the cartilage lacunae density and staining preservation. For the skin, the 3D volume confirmed the presence of intact dermal papillae and adnexal removal. The connective tissue, including deep dermis, adipose tissue, vessels and glands appeared at a lesser density. On the 3D volumes quantification, the porosity of whole-biopsy volume was increased in the decellularized sample, with a mean non-stained ratio to stained areas of $32.2 \pm 2.2\%$, compared to $20.8 \pm 2.6\%$ in the native sample (Fig. 4C). When excluding the cartilage, the porosity in HE-ECM was even higher, with 46%,

signifying the loss of structural volumes mainly located in the non-cartilaginous areas.

3.3.4. Mechanical properties

Ball burst testing of cartilage revealed an overall reduction of stiffness in decellularized (9.3 ± 8.4 N/mm, range 1.5–21.3) compared to native samples (18.4 ± 9.3 N/mm, range 4.4–30.2). This result demonstrates an overall reduction of the stiffness in the

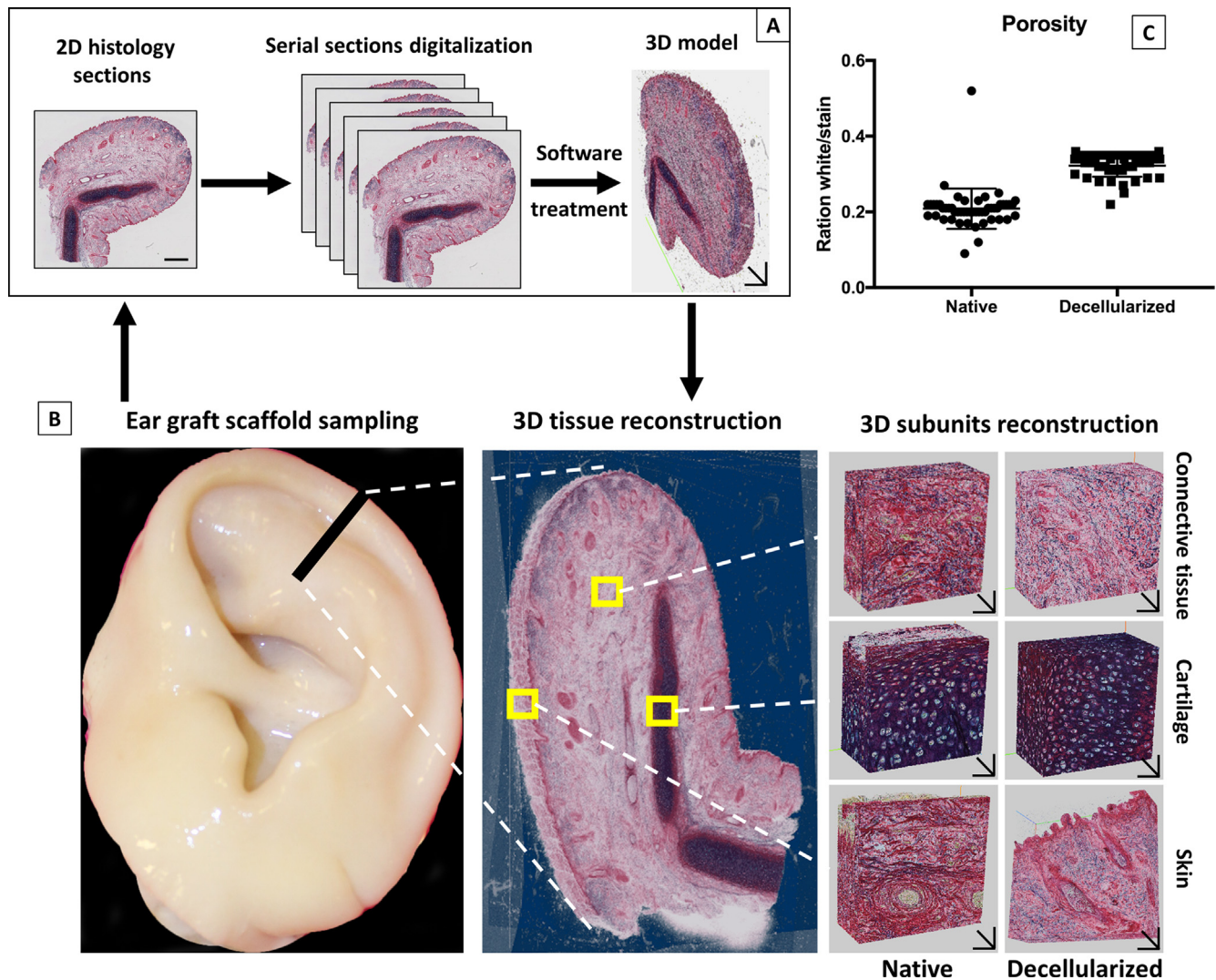


Fig. 4. ECM 3D-histology reconstruction. **A** Methodology: native and decellularized ear samples are serial sectioned, then digitalized and treated for 3D alignment and reconstruction with a specific software. 2D/3D scale bars: 1 mm. **B** Biopsy location (left), 3D-histology volume reconstruction and virtual sampling locations (middle) for 3D subunit elementary tissue reconstruction: connective tissue, cartilage and skin, from native and decellularized samples (right). 3D Scale bars: 75 μ m. **C** Porosity value calculated from the ratio between non-stained and stained area in the whole 3D biopsy volume from native and decellularized samples, with inclusion of cartilage layer.

decellularized group, remaining however in the same order of magnitude as for the native.

Tensile testing of skin showed an increase in maximum engineering stress after decellularization, along with an increase in dispersion of maximum stress (0.9+/-0.4 MPa for native tissues versus 1.2+/-0.6 MPa for decellularized tissues). Strain at maximum stress was not significantly different between native (0.4+/-0.1 MPa) and decellularized (0.4+/-0.2 MPa) tissues (See Supplementary material 3, skin stress-strain curves).

3.4. HE-ECM preservation of cytokines

The cytokine analysis revealed that essentially all 42 tested cytokines were measurable in skin, cartilage and fat samples. In order to quantitatively characterize cytokine preservation in the different tissues of the scaffold, we analyzed the degree of change of growth factors in each biological sample. As shown (Fig. 5A), all the measured cytokines in skin samples collected from the decellularized scaffold decreased significantly compared to native skin samples. Conversely, none of the measured cytokines decreased significantly by decellularization in fat tissue, with the exception of IL-4 which was below detection level. Cartilage pre-

sented a middle behavior with 22/44 cytokines significantly decreased after decellularization compared to controls. To better understand how the decellularization process affected cytokines in HE-ECM, we calculated the relative proportion of preservation for each cytokine in decellularized tissues expressed as percentage of the native mean abundance (Fig. 5B). In order to investigate whether different cytokine subclasses were differentially affected by the decellularization process, the following cytokine groups were created according to cytokine function: 1) pro-inflammatory cytokines (IL-1 β , IL-6, IFN γ , TNF- α , MIF), 2) Chemokines (IL-16, CCL1, CCL2, CCL3, CCL7, CCL8, CCL11, CCL13, CCL15, CCL17, CCL19, CCL20, CCL21, CCL22, CCL23, CCL24, CCL25, CCL26, CCL27, CXCL1, CXCL2, CXCL6, CXCL9, CXCL10, CXCL11) and 3) Growth factors (IL-2, IL-4, IL-8, IL-10, GM-CSF, TGF- β 1, TGF- β 2, TGF- β 3, CXCL5, CXCL12). Although many cytokines exhibit pleiotropy, we classified each cytokine into one of the three groups. No double classifications were allowed. As shown (Fig. 5C), in decellularized skin total protein preservation was 8.75 \pm 4.07% with similar preservation of pro-inflammatory cytokines and chemokines (5.88 \pm 5.0% and 7.13 \pm 7.87%, respectively). Growth factors showed a much higher percentage of preservation (152.6 \pm 213.84) compared to pro-inflammatory cytokines and chemo-

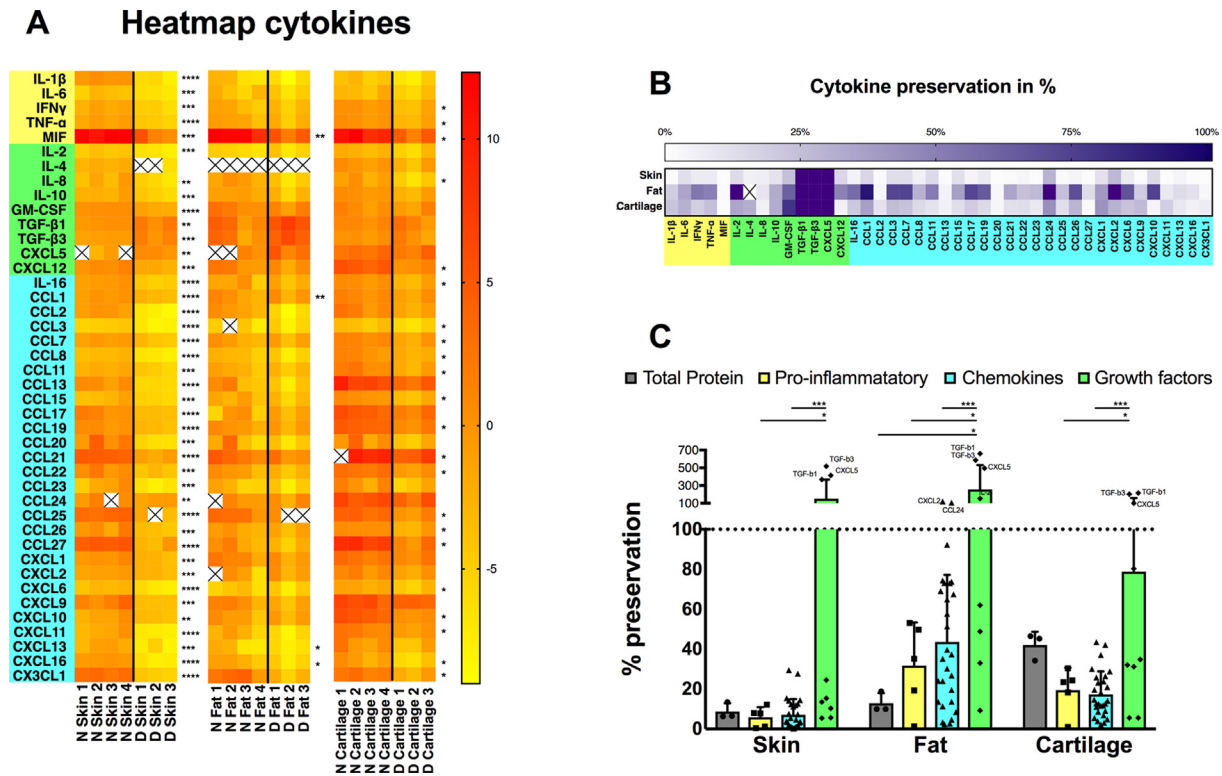


Fig. 5. Cytokines quantification. **A** Heatmap showing changes in abundances of 42 absolutely quantified cytokines in skin, fat and cartilage biopsies from four native (N-) and three decellularized (D-) scaffolds. Individual protein pictogram abundance per milligram of tissue was log₂ transformed. Yellow boxes correlate with lower protein concentration and red boxes with higher protein concentration (see scale). Crossed boxes indicate samples under the detection limit. *p < 0.05; **p < 0.01; ***p < 0.0001 by two-sample t-tests with Benjamini, Krieger and Yekutieli correction to compare native and decellularized values. **B** Heatmap showing cytokine preservation after decellularization in skin, fat and cartilage as percentage of native tissues abundance. White boxes correlate with lower preservation and blue boxes with higher cytokine preservation. Purple boxes indicate increased cytokine levels as compared to native tissues ($\geq 100\%$). **C** Relative preservation of total protein extract (grey), pro-inflammatory cytokines (yellow), chemokines (green) and growth factors (blue) in decellularized skin, fat and cartilage. Highly preserved cytokines (>100%) are indicated. Data presented as mean \pm SD. *p < 0.05; ***p < 0.001 by one-way ANOVA with Tukey's correction. (For interpretation of the references to color in this figure legend, the reader is referred to the web version of this article.)

kines. Similar results were observed in cartilage ($41.99 \pm 6.73\%$, $19.48 \pm 11.21\%$, $17.30 \pm 11.53\%$ and $78.77 \pm 80.37\%$ of preservation of total protein, pro-inflammatory cytokines, chemokines and growth factor, respectively) and in fat ($12.9 \pm 5.09\%$, $31.74 \pm 21.65\%$, $43.63 \pm 33.52\%$, $255.94 \pm 275.28\%$ of preservation of total protein, pro-inflammatory cytokines, chemokines and growth factor, respectively). Interestingly, only three of the forty-two cytokines (i.e., TGF- β 1, TGF- β 3 and CXCL5) showed an increase in expression levels when comparing decellularized and native tissues. This is likely due to more efficient protein extraction in the cell-empty ECMs and the increase in the ratio of pg cytokine per total ECMs weight in the decellularized tissues. In fat tissue, three cytokines displayed relative increase as compare to native tissue (i.e., IL-2, CXCL2 and CCL24), confirming the higher capacity of the adipose tissue to retain growth factors during the decellularization process. Apart from TGF- β 1, TGF- β 3 and CXCL5 the most preserved cytokines across tissues were IL-2, GM-CSF, CCL1, CCL24 and CXCL2 (Fig. 5B).

3.5. In vivo implantation – Biocompatibility study

There was no adverse event encountered at the time of graft implantation. During scaffold retrieval, the surrounding abdominal wall skin appeared healthy, and after incision and direct implant observation, no obvious capsular formation could be identified. The integration with recipient tissues was satisfying in all groups with signs of macroscopic vascular infiltration present. At histology, the cellular infiltration was diffuse at POD15 and POD30, but less important at POD60, with signs of micro-vascular perme-

ability in the deep scaffold (Fig. 6A), compared to the native control (Fig. 6A and B), even the difference was not as strong as expected, due to the sterilization protocol. Remodeling was globally limited. CD68 + macrophage infiltration was significant and located exclusively within the scaffold, being less intense and more peripheral at POD60 (Fig. 6C–F); this correlates to the CD68 staining quantification, in which the % stained area was significantly ($p < 0.0001$) higher in the control native group at POD15, with reduction at POD30 so that there was now no difference between groups. At POD60, the native group was significantly more infiltrated than the decellularized group (**p < 0.001). Interestingly, the decellularized group was significantly less infiltrated at POD60 compared to the same group at POD30 (Fig. 6G). Regarding qualitative and quantitative anti-CD3 staining, response was found very poor, in both native and decellularized samples, mainly located at the surface of the scaffolds, and without great difference between groups. Flow cytometry of circulating rat anti-human IgG antibodies showed the following positive recipient immunization: 2/3 POD15 and POD30, 2/2 POD60 in control group, compared to 0/3 POD15, 1/3 POD30 and 0/2 POD60 (Fig. 6H, see Supplementary material 4).

3.6. In vitro compatibility

For rASCs-seeded scaffolds, MTT staining revealed homogeneous engraftment of viable cells on all scaffolds. On the full-thickness scaffolds, cells were located on all tissue layers including the epidermal side (Fig. 7A–C). Cell viability was confirmed by live/dead staining, with a few dead cells identified (Fig. 7D–F).

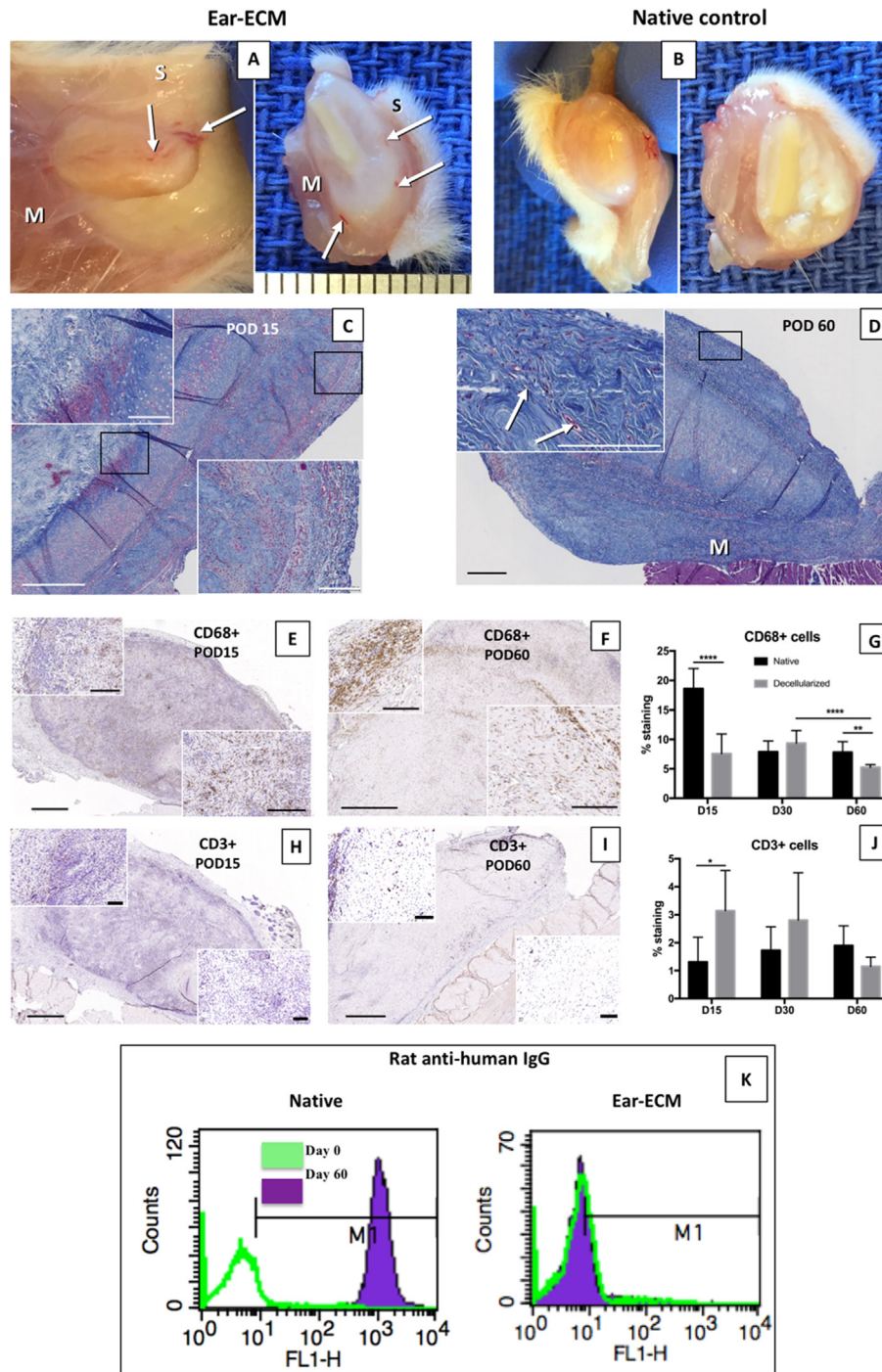


Fig. 6. In vivo study, subcutaneous implantation in rat. **A and B** Macroscopic assessment: **A** HE-ECM implant at time of explantation, external aspect (left) and section aspect (right) integration between layers of skin (S) and muscle (M) of the recipient's abdominal wall, with no signs of capsular formation and evidence of growing vessels (arrows); **B** Comparison with native control with more although limited peripheral reaction (left) and absence of neo-vessels at section inspection (right); **C-D** HE-ECM Masson's trichrome assessment at **C** postoperative day POD15 and **D** POD60, with diminution of cellular infiltration, limited remodeling and patent blood vessels (arrows in **D** insert). M Muscle. **E-F** Macrophage infiltration CD68 IHC staining at **E** POD15, **F** POD60; windows enlarged views in the inserts. **G** CD68 quantification at POD15, POD30 and POD60 in native (black) and decellularized (grey) implants; **H-I** Lymphocyte infiltration CD3 IHC staining at **H** POD15, **I** POD60; windows enlarged views in the inserts. **J** CD3 quantification at POD15, POD30 and POD60 in native (black) and decellularized (grey) implants; **K** Flow cytometry of anti-human circulating IgG antibodies in the rat recipient at D0 (green curve) and POD60 (purple curve), in native (above) and decellularized (below) recipients. Selected curves originate from the most representative positive (control) and negative (decellularized) flow cytometries (for complete data set, see supplementary Fig. 3). $\dagger p < 0.05$; $\dagger\dagger p < 0.001$; $\dagger\dagger\dagger p < 0.0001$. Scale bars: 1 mm in overview section, 200 μ m in inserts. (For interpretation of the references to color in this figure legend, the reader is referred to the web version of this article.)

3.7. Whole-ear perfusion-bioreactor seeding

No sign of contamination was recorded during the experiment. At retrieval, the cultured HE-ECM appeared diffusely pink, indicating perfusion and impregnation of the culture medium (Fig. 8A–C).

CD31 staining was positive (to be compared with Fig. 2D) on the endothelial wall of vessels from various calibers, found both in superficial and deep part of the scaffold. Live/dead staining show intra-vascular distribution of living cells, in small and larger vessels (Fig. 8). However, no cell nuclei could be observed with

Rat adipose-derived stem cells

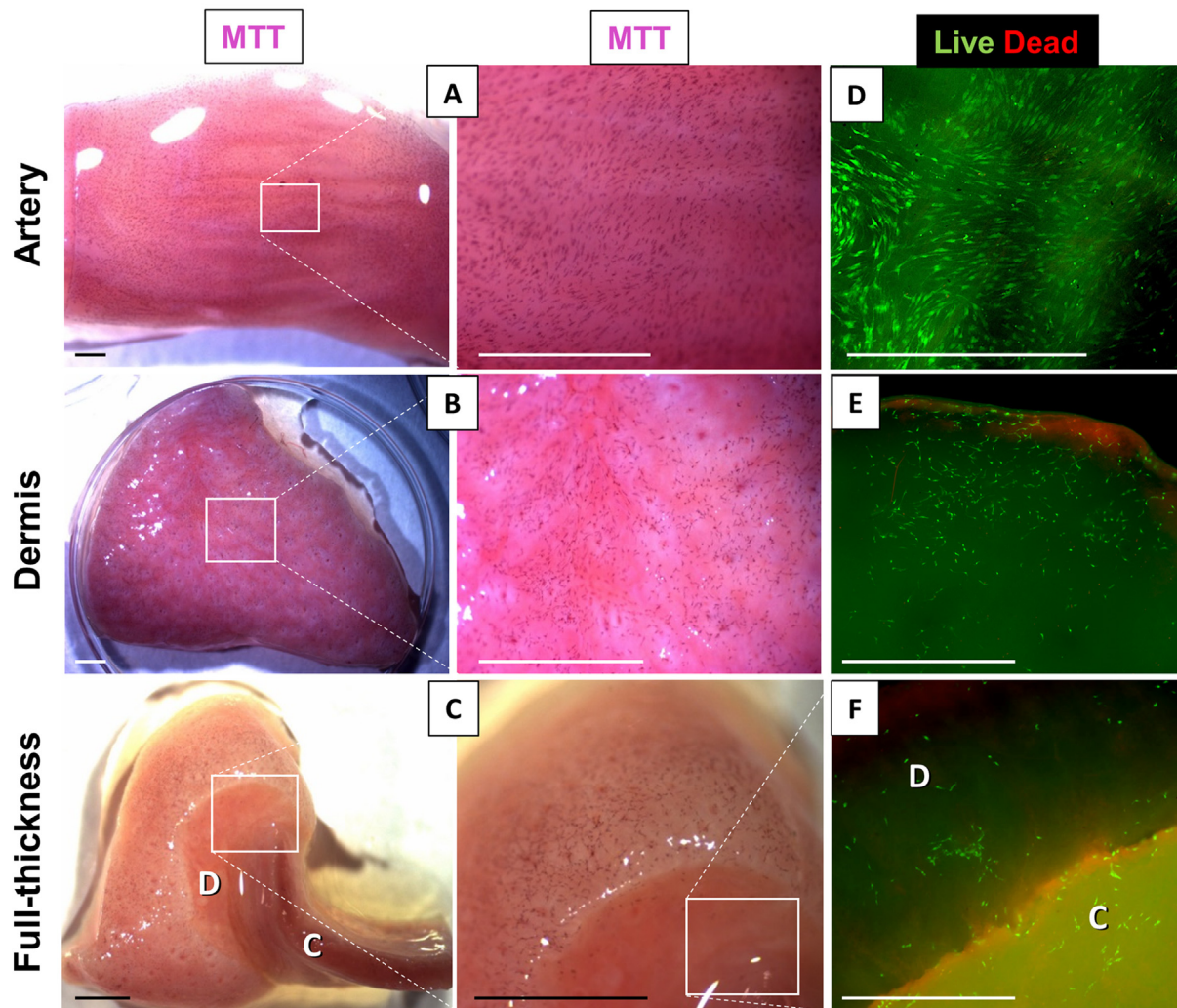


Fig. 7. *In vitro* compatibility. Static seeding with rat adipose-derived Stem Cells (ASC) 3.6×10^4 cells/cm² for 14 days: **A–C** Seeded scaffold and enlarged view, and observation of MTT staining, **D–F** Live/dead vital staining examination on whole-mount, of arterial pedicle (upper row), dermis (middle row) and full-thickness (lower row) samples from HE-ECM; **D** dermis, **C** cartilage. Scale bars: 1 mm.

H&E staining in the large pedicles, either in the lumen or the vessels endothelial surface (see Supplementary Fig. 5). Finally, whole-mount MTT vital staining allow to appreciate the seeding cover, even if segmental, of the scaffold vascular tree (Fig. 8F).

4. Discussion

A functional, implantable and clinically applicable engineered auricle is our ultimate objective. This study takes important steps in achieving this goal. We were able to produce whole acellular human ears with route for access to the vascular tree utilizing the approach of Vascularized Composite tissue Engineering. We demonstrated that early findings from porcine ear engineering [18] could be applicable to a human auricular graft model, confirming the relevance of the pig model in a preclinical experimental approach for composite tissue engineering. The feasibility of using elderly postmortem human donors, even several days after death, was shown. This is possible because of high collagen content of composite tissue ECM that seems to better handle cell necrosis and proteolytic enzymes, likely due to the presence of cell populations with low metabolic activity and less aggressive enzymatic

content, as compared to exocrine pancreas cells involving complex organ engineering challenges [27]. Finally, vascular tree patency was displayed at all levels throughout the auricular ECM scaffold. It is however important to highlight that a diseased vascular tree, with extensive arteriosclerosis, can compromise perfusion and thus success in the decellularization.

An important difference when comparing the present data with our porcine ear study concerned the adipose tissue defatting: the ability to remove nuclei was efficient with detergents, as confirmed by DAPI staining, but a high content of scattered oil cysts persisted, requiring an additional treatment with polar solvent, as recommended in non-perfused isolated human adipose tissue engineering [22]. Our polar solvent step resulted in successful fat removal, although DAPI staining showed nuclei removal prior to the step, without impairment of the vascular tree. Even if considered as a minor issue for organ bioengineering, the ability to completely treat the adipose tissue is critical when dealing with composite tissue engineering, as fat represents a major component for this type of graft, in both qualitative and quantitative aspects. The real question however is whether adipose tissue needs to be fully treated or not, as the use polar solvent is not straightforward. When considering

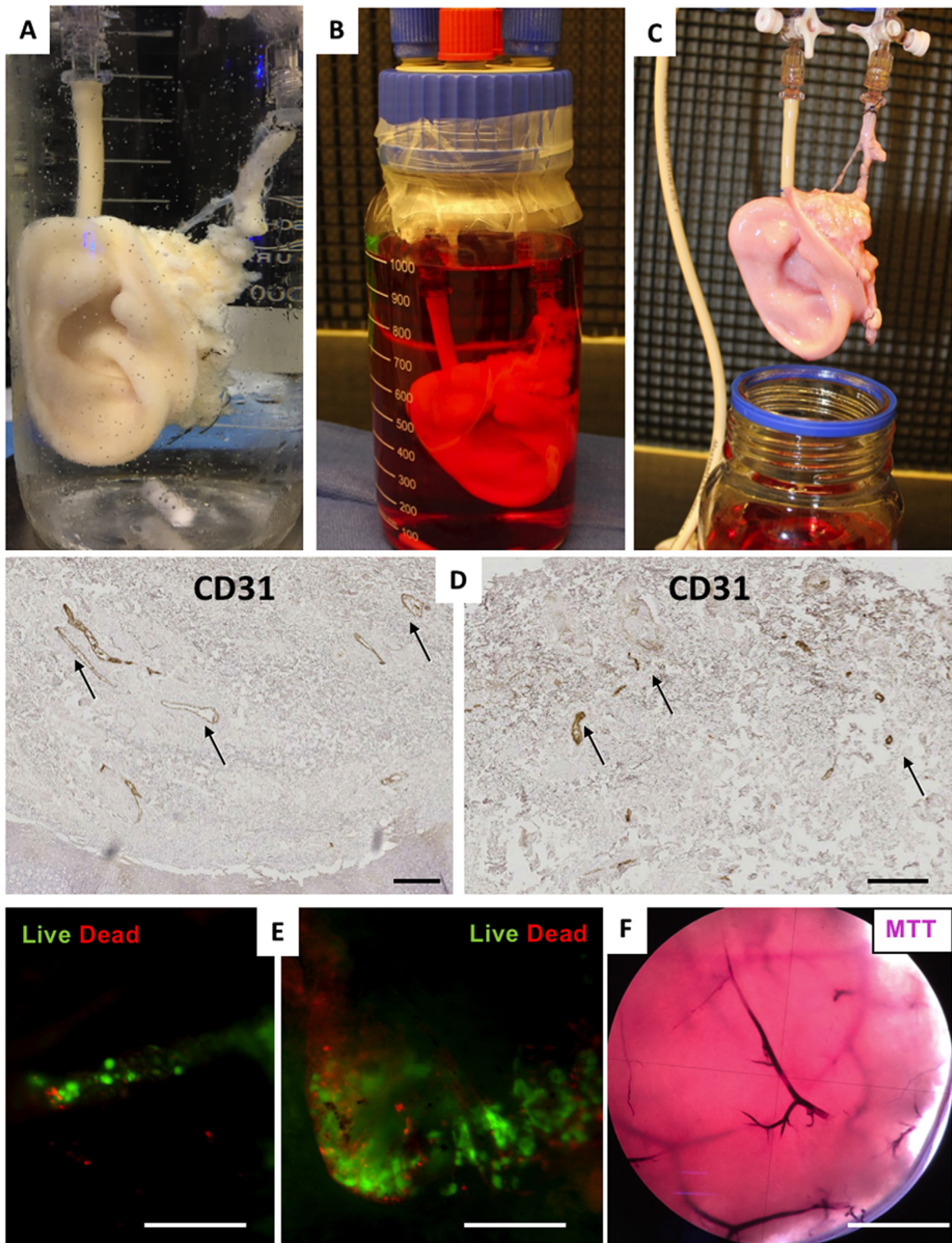


Fig. 8. Whole-ear scaffold perfusion-bioreactor seeding. **A** Perfusion-sterilization with 0.1% peracetic acid and PBS rinsing. **B** Sterile mounting in perfusion-bioreactor, and immersion with culture medium, prior to cell seeding **C** Ear graft scaffold at time of retrieval, with pinky aspect as sign of proper culture medium perfusion and ECM impregnation. **D** CD31 staining positivity (arrows), in deep (left) and superficial (right) scaffold structure. **E-F** Whole-mount staining and direct microscope observation after **E** Live/dead and **F** MTT vital stainings. Scale bars: 200 μ m, with exception of MTT observation with microscope 10x magnification: 1 mm.

in vivo application, persistence of lipid droplets can trigger a significant inflammatory reaction that may be deleterious to scaffold implantation. Moreover, even for *in vitro* application only, native adipose tissue persistence results in reduced engraftment of new

adipocyte and thus poorer adipose tissue regeneration [23]. This illustrates the need for combination of decellularizing agents in VCE. Indeed, other tissues were successfully treated, with only some donor cells observed in the cartilage. These few remaining

cells should not be an issue considering the significant reduction of total DNA observed in this tissue and its poor immunogenicity due to its avascular nature and ECM density [15].

Following processing, the auricular ECM structural components and 3D organization were well-preserved, which is critical for body parts in which function is directly related to the preservation of its form. The stiffness of the decellularized cartilage was maintained in an acceptable manner in our study, which applies directly to the target function of shape preservation of TE auricles, but may not be universally applicable to other tissue such as knee articular cartilage which experiences repetitive strain as its main function. Due to the cadaveric origin and the variability of the donors in this study, such results provide an overall appreciation of such an assessment. In order to further determine the structural organization of the auricular VCE, we performed a 3D characterization. This innovative tool brings a new level of resolution to scaffold analysis, allowing for precise comprehension of the spatial organization of both native and decellularized tissue with accurate reproduction of ECM in tissue engineering. As a quantitative measurement, porosity was calculated based on 3D volume, which is a more accurate assessment than conventional 2D analysis can provide. Still, new 3D analytic tools need to be developed for soft tissue and organ engineering evaluation, so as to mimic the success of 3D bone tissue evaluation [28].

Perfusion-decellularization with SDS-based protocol seems to be suitable for protection of innate cytokines of skin, fat and cartilage in the human ear. We showed that cytokines of different function and nature are preserved to a measurable extent. Overall, growth-inducing cytokines were preserved most frequently, followed by the cell-guiding chemokines then inflammatory cytokines. It has been previously demonstrated that growth factors such as TGF- β , VEGF, and bFGF are present in acellular ECM scaffolds, and these growth factors retain most of their biologic activity following decellularization of the ECM and therefore may contribute to the favorable characteristics of decellularized ECM scaffolds [29–32]. In our study we demonstrate a better preservation of “protective” growth factors and a more pronounced depletion of pro-inflammatory cytokines across all analyzed tissues. In addition to the positive cytokine profile, we also observed distinct responses to the perfusion process of individual tissue ECMs in terms of protein preservation, with cartilage and fat being the most preserved tissues. Taken together, these findings suggest that newly colonizing cells in the ECM scaffold may benefit of the presence of preserved growth factors bounded to the ECM and that ECM obtained via perfusion-decellularization are therefore very likely to increase the success rate of cell-reseeding. However, in this study we did not assess the biological activity of the measured cytokines. Considering the nature of the decellularization protocol it is possible that not all the measured cytokines will be biologically active and some of them would be in a denatured and inactive form. It cannot be rule out that these denatured cytokines may stimulate immune response against the scaffold. Future studies are warranted to assess the how the specific components (both structural and soluble) retained within an ECM scaffolds may activate the immune response and to verify whether, as recently proposed, acellular ECM scaffolds may modulate the host immune response towards a functional tissue replacement outcome [32].

We observed an overall increase of vascular resistances during scaffold production, especially during SDS perfusion. This phenomenon of increasing vascular pressure during perfusion-decellularization has been described for other organs [17,33] with a subsequent decrease in resistance after re-endothelialization. In contrast to these findings, MAP was already back to normal values after PBS rinsing in our study. Considering adaptation of perfusion inflow, we question the need to adapt flow to follow constant ideal vascular resistance, as recommended for solid organs preservation

and engineering. Indeed, during the initial steps, a high pressure increases the risk of damage to microcirculation and of edema formation. Furthermore, vascular resistances after cellular depletion likely reflect extra-vascular rigidity with subsequent increased pressures against flow. Thus, maintaining adequate flow, against increased vascular resistances, should be the goal to allow distal perfusion.

During the *in vivo* part of our study, the decellularized scaffolds were well tolerated even when significant remodeling was observed, with an important CD68 + macrophage infiltration during the first 8 weeks post-implantation. This remodeling is well-known [34,35] and part of a necessary integration period of the ECM by the recipient, with a related ECM mass decrease. In our study, we observed a preservation of the ECM structure at POD60, with less remodeling than expected for an ECM rich in collagen. The discrepancies observed when screening anti-donor circulating IgG may rely on the immunogenicity of the treated ECM itself, along with the use of cadaveric donors. For the control, the immune response was mild, explained by the need to use non-fresh controls from human cadavers, with reduced allogenic properties. This was even more obvious on the anti-CD3 qualitative and quantitative assessments, with a very light difference between decellularized and native groups. Moreover, the need to sterilize native tissues with 0.1% PCA participated in reducing allogenicity further, as PCA itself has been described as a decellularizing agent on its own [36]. This illustrates the need in such studies to use more sophisticated techniques as FACS and antibody detection, to draw conclusions about immune response. This appears to be the downside of using human grafts from cadaveric sources, and further studies should investigate the effect of procurement delay and conditions on the overall outcome and immune response *in vivo*. Nevertheless, this model is a very useful tool to study and establish VCE protocols at a direct human scale, with readily accessible donor supply.

When dealing with future whole-graft scaffold recellularization strategies, it is of paramount importance to consider the ear as a complex 3D anatomical structure at all scales, with multilayered tissues including skin, cartilage, fat, nerves and blood vessels. This conceptual framework highlights the challenges of creating a clinically useful auricle graft based on conventional TE approaches, to provide the expected complexity of the living associated to a transplantable vascular tree, to allow the survival of the engineered ear. Even if we had an efficient protocol readily available to adequately treat all the tissues at once to produce a decellularized ECM scaffold with a single vascular access, recellularization remains an important problem to solve. As demonstrated in this study, vascular access to facilitate seed dissemination and preservation of basal membranes are prerequisite factors to allow dermal perfusion of culture medium with subsequent cell engraftment; non-perfused TE skin construct approaches are limited in their ability to recellularize a scaffold [37]. Apart from skin and vessels, which can be approached in a direct manner for seeding, other tissue types, such as cartilage and adipose, are buried deep in the scaffold, making it almost impossible for any selective seeding like topical, vascular injection, or cell infusion. For these tissues, the ideal option relies on a single-type stem cell approach, that differentiates and replicates when in contact with specific ECM tissues, as demonstrated by other groups [38,39]. For the cartilage, combined to a whole composite scaffold, like ear or nose, the difficulty will be important, by its deep location in the graft and the absence of vascular access. The current strategies in cartilage engineering have successfully treated isolated scaffolds [7,40], but cannot be directly applied to our cadaveric auricular ECM scaffold model at this time. Perichondrium and peripheral cartilage enhanced porosity could allow seeded cells to repopulate the decellular-

ized cartilage adequately with further research efforts. The different whole-ear bioreactor seeding experiments we performed showed that the step of cadaveric human ear recellularization step can be reached with our current approach; we still need to improve the cell choices, the cells engraftment strategies, relying on perfusion-seeding methodology as well as the number of cells available *in vitro*. Regarding, this last point, we already know that, even for such a small graft, the number of cells needed will be prohibitive; the most pertinent strategies will be very likely to combine partial *in vitro* seeding and *in vivo* maturation of the scaffold. For all these reasons, the main key to success is the long-term vascular reperfusion in a recipient, a shared limitation with parallel organ bioengineering strategies. But once a reliable vascular regeneration methodology will be available, the clinical applications, especially in a study already at the scale of human grafts, will be straight-forward.

5. Conclusions

Complex auricular scaffolds with preserved vasculature can be obtained from human delayed postmortem sources to provide a platform for further functional tissue engineered constructs. Access to an auricular vascular tree, for which preservation and accessibility has been obtained for the first time in this study, is the key step required to translate experimental science to clinical usage. Overall, perfusion-decellularization application to body parts show great promise in generating suitable composite tissue scaffolds for body reconstruction. The goal of future experiments should be to improve the efficiency of the decellularization protocol and to improve recellularization by enhancing vascular seeded engraftment and density, as well as epidermal regeneration on a perfused acellular dermis.

Author contributions

JD designed study, performed all procurements, set up and performed all decellularizations and scaffolds seeding, interpreted data, wrote article. HA and DA participated extensively to specimen collection and treatment, performed analysis. TW, AT, EV and RR performed all cytokines quantifications. CBo performed all histological processing and quantifications. DM was responsible for 3D histology reconstruction and quantification. VD and PD performed all mechanical testings. DH and GO participated to study design and data interpretation. CBe, PG and BL participated to study design, supported all analysis. All authors interpreted data, revised manuscript and gave their final approval.

Acknowledgments

The authors express gratitude to Erick Montoya, An Catherine Hoang Le Thien, Sarah El Hathout, Daela Xhema, Marc de Bournonville, Darren Treanor, Chantal Fregimilicka, Michele De Beukelaer, Christine de Ville de Goyet, Marie Henry, Bernard Caalen, Pascale Segers and Walter Hudders for their devoted technical assistance or logistic support. Finally, the authors thank Alain Despont for his valuable and extensive support for the Luminex assay.

Conflict of interest/disclosure

HG-MIM Software is produced by HeteroGenius Limited, UK, of which Derek Magee is a director. All authors approved the final version of the article.

Funding source

This work was supported by a Fondation Saint-Luc Grant, FSR-UCL (Fonds Spécial de la Recherche) and Fonds Dr. Gaëtan Lagneaux.

Appendix A. Supplementary data

Supplementary data associated with this article can be found, in the online version, at <https://doi.org/10.1016/j.actbio.2018.04.009>.

References

- [1] F. Firmin, A. Marchac, A novel algorithm for autologous ear reconstruction, *Semin. Plast. Surg.* 25 (2011) 257–264.
- [2] L. Kasrai, A.K. Snyder-Warwick, D.M. Fisher, Single-stage autologous ear reconstruction for microtia, *Plast. Reconstr. Surg.* 133 (2014) 652–662.
- [3] S. Nagata, A new method of total reconstruction of the auricle for microtia, *Plast. Reconstr. Surg.* 92 (1993) 187–201.
- [4] N. Baluch, S. Nagata, C. Park, G.H. Wilkes, J. Reinisch, L. Kasrai, D. Fisher, Auricular reconstruction for microtia: a review of available methods, *Plast. Surg. (Oakv.)* 22 (2014) 39–43.
- [5] J.P. Giot, D. Labbe, E. Soubeyrand, R. Pacini, M.R. Guillou-Jamard, J.F. Compere, H. Benateau, Prosthetic reconstruction of the auricle: indications, techniques, and results, *Semin. Plast. Surg.* 25 (2011) 265–272.
- [6] B.G. Lengelé, Current concepts and future challenges in facial transplantation, *Clin. Plast. Surg.* 36 (2009) 507–521.
- [7] Y. Cao, J.P. Vacanti, K.T. Paige, J. Upton, C.A. Vacanti, Transplantation of chondrocytes utilizing a polymer-cell construct to produce tissue-engineered cartilage in the shape of a human ear, *Plast. Reconstr. Surg.* 100 (1997) 297–302.
- [8] H.W. Kang, S.J. Lee, I.K. Ko, C. Kengla, J.J. Yoo, A. Atala, A 3D bioprinting system to produce human-scale tissue constructs with structural integrity, *Nat. Biotechnol.* 34 (2016) 312–319.
- [9] T.M. Cervantes, E.K. Bassett, A. Tseng, A. Kimura, N. Roscioli, M.A. Randolph, J.P. Vacanti, T.A. Hadlock, R. Gupta, I. Pomerantseva, C.A. Sundback, Design of composite scaffolds and three-dimensional shape analysis for tissue-engineered ear, *J. R. Soc. Interface* 10 (2013) 20130413.
- [10] H.C. Ott, B. Clippinger, C. Conrad, C. Schuetz, I. Pomerantseva, L. Ikonoumou, D. Kotton, J.P. Vacanti, Regeneration and orthotopic transplantation of a bioartificial lung, *Nat. Med.* 16 (2010) 927–933.
- [11] H.C. Ott, T.S. Matthiesen, S.K. Goh, L.D. Black, S.M. Kren, T.I. Netoff, D.A. Taylor, Perfusion-decellularized matrix: using nature's platform to engineer a bioartificial heart, *Nat. Med.* 14 (2008) 213–221.
- [12] G. Orlando, A.C. Farney, S.S. Iskandar, S.H. Mirmalek-Sani, D.C. Sullivan, E. Moran, T. Aboushwareb, P. De Coppi, K.J. Wood, R.J. Stratta, A. Atala, J.J. Yoo, S. Soker, Production and implantation of renal extracellular matrix scaffolds from porcine kidneys as a platform for renal bioengineering investigations, *Ann. Surg.* 256 (2012) 363–370.
- [13] G. Orlando, S. Soker, R.J. Stratta, Organ bioengineering and regeneration as the new Holy Grail for organ transplantation, *Ann. Surg.* 258 (2013) 221–232.
- [14] B.E. Uygun, G. Price, N. Saedi, M.L. Izamis, T. Berendsen, M. Yarmush, K. Uygun, Decellularization and recellularization of whole livers, *J. Vis. Exp.* (2011).
- [15] N. Hou, P. Cui, J. Luo, R. Ma, L. Zhu, Tissue-engineered larynx using perfusion-decellularized technique and mesenchymal stem cells in a rabbit model, *Acta Otolaryngol.* 131 (2011) 645–652.
- [16] R. Ma, M. Li, J. Luo, H. Yu, Y. Sun, S. Cheng, P. Cui, Structural integrity, ECM components and immunogenicity of decellularized laryngeal scaffold with preserved cartilage, *Biomaterials* 34 (2013) 1790–1798.
- [17] B.J. Jank, L. Xiong, P.T. Moser, J.P. Guyette, X. Ren, C.L. Cetrulo, D.A. Leonard, L. Fernandez, S.P. Fagan, H.C. Ott, Engineered composite tissue as a bioartificial limb graft, *Biomaterials* 61 (2015) 246–256.
- [18] J. Duisit, G. Orlando, D. Debluts, L. Maistriaux, D. Xhema, Y.A. de Bisthoven, C. Galli, A. Peloso, C. Behets, B. Lengelé, P. Gianello, Decellularization of the porcine ear generates a biocompatible, nonimmunogenic extracellular matrix platform for face subunit bioengineering, *Ann. Surg.* 266 (2017) 754–764.
- [19] J. Duisit, L. Maistriaux, A. Taddeo, G. Orlando, V. Joris, E. Coche, C. Behets, J. Lerut, C. Dessy, G. Cossu, E. Vögelin, R. Rieben, P. Gianello, B. Lengelé, Bioengineering a human graft: the matrix of Identity, *Ann. Surg.* (2017) [Epub ahead of print].
- [20] B.G. Ulusal, A.E. Ulusal, J.Y. Lin, B.K. Tan, C.H. Wong, C. Song, F.C. Wei, Anatomical and technical aspects of harvesting the auricle as a neurovascular facial subunit transplant in humans, *Plast. Reconstr. Surg.* 120 (2007) 1540–1545.
- [21] J. Duisit, H. Amiel, D. Debluts, L. Maistriaux, A. Gerdom, A. Bol, P. Gianello, C. Behets, B. Lengelé, Single-artery human ear graft procurement: a simplified approach, *Plast. Reconstr. Surg.* 140 (2017) 599–603.
- [22] L.E. Flynn, The use of decellularized adipose tissue to provide an inductive microenvironment for the adipogenic differentiation of human adipose-derived stem cells, *Biomaterials* 31 (2010) 4715–4724.

- [23] L. Wang, J.A. Johnson, Q. Zhang, E.K. Beahm, Combining decellularized human adipose tissue extracellular matrix and adipose-derived stem cells for adipose tissue engineering, *Acta Biomater.* 9 (2013) 8921–8931.
- [24] P. Sarathchandra, R.T. Smolenski, A.H. Yuen, A.H. Chester, S. Goldstein, A.E. Heacox, M.H. Yacoub, P.M. Taylor, Impact of gamma-irradiation on extracellular matrix of porcine pulmonary valves, *J. Surg. Res.* 176 (2012) 376–385.
- [25] C.A. Schneider, W.S. Rasband, K.W. Eliceiri, NIH Image to ImageJ: 25 years of image analysis, *Nat. Methods* 9 (2012) 671–675.
- [26] T. Schubert, D. Xhema, S. Veriter, M. Schubert, C. Behets, C. Delloye, P. Gianello, D. Dufrane, The enhanced performance of bone allografts using osteogenic-differentiated adipose-derived mesenchymal stem cells, *Biomaterials* 32 (2011) 8880–8891.
- [27] A. Peloso, L. Urbani, P. Cravedi, R. Katari, P. Maghsoudlou, M.E. Fallas, V. Sordi, A. Citro, C. Purroy, G. Niu, J.P. McQuilling, S. Sittadjody, A.C. Farney, S.S. Iskandar, J.P. Zambon, J. Rogers, R.J. Stratta, E.C. Opara, L. Piemonti, C.M. Furdui, S. Soker, P. De Coppi, G. Orlando, The human pancreas as a source of protolerogenic extracellular matrix scaffold for a new-generation bioartificial endocrine pancreas, *Ann. Surg.* 264 (2016) 169–179.
- [28] D. Chappard, E. Legrand, B. Haettich, G. Chales, B. Auvinet, J.P. Eschard, J.P. Hamelin, M.F. Basle, M. Audran, Fractal dimension of trabecular bone: comparison of three histomorphometric computed techniques for measuring the architectural two-dimensional complexity, *J. Pathol.* 195 (2001) 515–521.
- [29] S.L. Voytik-Harbin, A.O. Brightman, M.R. Kraine, B. Waisner, S.F. Badylak, Identification of extractable growth factors from small intestinal submucosa, *J. Cell. Biochem.* 67 (1997) 478–491.
- [30] C.A. McDevitt, G.M. Wildey, R.M. Cutrone, Transforming growth factor-beta1 in a sterilized tissue derived from the pig small intestine submucosa, *J. Biomed. Mater. Res. A* 67 (2003) 637–640.
- [31] J.P. Hodde, D.M. Ernst, M.C. Hiles, An investigation of the long-term bioactivity of endogenous growth factor in OASIS Wound Matrix, *J. Wound Care* 14 (2005) 23–25.
- [32] J.L. Dziki, L. Huleihel, M.E. Scarritt, S.F. Badylak, Extracellular matrix bioscaffolds as immunomodulatory biomaterials, *Tissue Eng. Part A* 23 (2017) 1152–1159.
- [33] J.J. Song, J.P. Guyette, S.E. Gilpin, G. Gonzalez, J.P. Vacanti, H.C. Ott, Regeneration and experimental orthotopic transplantation of a bioengineered kidney, *Nat. Med.* 19 (2013) 646–651.
- [34] B.E. Uygun, A. Soto-Gutierrez, H. Yagi, M.L. Izamis, M.A. Guzzardi, C. Shulman, J. Milwid, N. Kobayashi, A. Tilles, F. Berthiaume, M. Hertl, Y. Nahmias, M.L. Yarmush, K. Uygun, Organ reengineering through development of a transplantable recellularized liver graft using decellularized liver matrix, *Nat. Med.* 16 (2010) 814–820.
- [35] S.F. Badylak, T.W. Gilbert, Immune response to biologic scaffold materials, *Semin. Immunol.* 20 (2008) 109–116.
- [36] P.M. Crapo, T.W. Gilbert, S.F. Badylak, An overview of tissue and whole organ decellularization processes, *Biomaterials* 32 (2011) 3233–3243.
- [37] H. Bannasch, G.B. Stark, F. Knam, R.E. Horch, M. Fohn, Decellularized dermis in combination with cultivated keratinocytes in a short- and long-term animal experimental investigation, *J. Eur. Acad. Dermatol. Venereol.* 22 (2008) 41–49.
- [38] S.L. Ng, K. Narayanan, S. Gao, A.C. Wan, Lineage restricted progenitors for the repopulation of decellularized heart, *Biomaterials* 32 (2011) 7571–7580.
- [39] L. Cui, Y. Wu, L. Cen, H. Zhou, S. Yin, G. Liu, W. Liu, Y. Cao, Repair of articular cartilage defect in non-weight bearing areas using adipose derived stem cells loaded polyglycolic acid mesh, *Biomaterials* 30 (2009) 2683–2693.
- [40] I. Fulco, S. Miot, M.D. Haug, A. Barbero, A. Wixmerten, S. Feliciano, F. Wolf, G. Jundt, A. Marsano, J. Farhadi, M. Heberer, M. Jakob, D.J. Schaefer, I. Martin, Engineered autologous cartilage tissue for nasal reconstruction after tumour resection: an observational first-in-human trial, *Lancet* 384 (2014) 337–346.